Journal of Molecular Structure 1225 (2021) 129089

Contents lists available at ScienceDirect

Journal of Molecular Structure

journal homepage: www.elsevier.com/locate/molstr

Synthesis, Crystal structure and DFT studies of Polyfunctionalized Alkenes: A transition Metal-Free C(sp^2)-H Sulfenylation of electron deficient Alkyne

Mohit Saroha [a,b], Jayant Sindhu [c,*], Parvin Kumar [d], J.M. Khurana [a]

[a] Department of Chemistry, DCRUST, Murthal, Sonipat, 131001 India
[b] Department of Chemistry, University of Delhi, Delhi 110007
[c] Department of Chemistry, COBS&H, CCS Haryana Agricultural University, Hisar 125004
[d] Department of Chemistry, Kurukshetra University, Kurukshetra 136119

ARTICLE INFO

Article history:
Received 16 April 2020
Revised 5 August 2020
Accepted 14 August 2020
Available online 17 August 2020

Keywords:
Transition metal-free
DFT
Hirshfeld
Fingerprint
NBO
NLO
Fukui function

ABSTRACT

An efficient, novel and transition metal-free protocol has been developed for the synthesis of polyfunctionalized aminothioalkenes *via* direct C–H sulfenylation of *in situ* generated enamines. The reaction was performed using a catalytic amount of inexpensive and nontoxic K_2CO_3 under mild reaction condition. All the reactions resulted in good to excellent yields. The cross-coupling reaction has been achieved by *in situ* aerobic oxidation at room temperature with good functional group tolerance. The molecular architecture and stereochemistry has been established by spectral data, X-ray single crystal diffraction studies and supported by Density Functional theory (DFT). Hirshfeld surface analysis has been used to explore the intramolecular and intermolecular interactions present in the case of **4a**. Moreover, the intramolecular hyperconjugative interactions have been investigated using natural bond orbitals (NBOs) analysis and their intensity was categorized according to their second-order stabilization energy (E(2)). The electrostatic properties such as global reactivity descriptors, local reactivity descriptors, ESP and NLO have been investigated using DFT method and B3LYP/6–311+*G*(d) level of theory.

1. Introduction

Development of novel, green and accessible procedures for the synthesis polyfunctionalized functionalities is a worthwhile contribution in organic synthesis. The progression of new C-S cross-dehydrogenative coupling (CDC) strategies attract synthetic organic chemists due to wide application of organosulfur compounds in pharmaceuticals, agrochemicals, organic dyes, and materials chemistry [1–6]. The C–H activation is a class of organic transformations [7–9], wherein the Heck reaction has established itself with high practicality [10,11]. Lately, the cross-coupling (CC) reaction of aryl halides with aryl thiols has become one of the most efficient method for C-S bond formation. A number of CDC reactions have been developed recently to form C_{sp}-C_{sp}, C_{sp}-C_{sp}^2 and C_{sp}^2-C_{sp}^2 bonds [12–19]. With the focus on emergence of "*atom-economy*" [20,21] and "*green chemistry*"[22] in organic synthesis, transition metal-free functionalization and specially, the C–C and C-X bond formation *via* C–H activation or CDC reactions has become more important.

Several CDC reaction based methodologies have been developed for thiolation/sulfenylation *via* C–H activation which, however, require synthesis of thiolation reagents initially [23–31]. Direct utilization of arylthiols as sulfenylating agent in metal-free protocols have not been explored to a significant extent. Thiolation/sulfenylation of five and six membered heterocycles has been reported using transition metal-free reagents *viz.* I_2/BSA [32], K_2CO_3/DMSO [33], I_2/DMSO [34], *N*-chlorosuccinimide [35], I_2/DMSO [36], and $KClO_3$/ethylacetate [37]. Molecular oxygen has been utilized as mild oxidant in organic synthesis by various research groups in C–H oxygenation [38], C–H amination [39] and C–H thiolation of enamines/enaminones [40,41]. To the best of our knowledge, synthesis of polyfunctionalized alkenes *via* CDC mediated sulfenylation of enamines by using environmentally benign method has not been explored yet.

The non-covalent interactions largely affect the molecular architecture by controlling the aggregation process in crystals. [42] The role of strong hydrogen bonds (O—H••••O, N—H••••H, N—H••••O etc.) is very significant in crystal packing [43]. Further, crystal pack-

* Corresponding author.
E-mail addresses: jayantchem@gmail.com (J. Sindhu), jmkhurana1@yahoo.co.in (J.M. Khurana).

https://doi.org/10.1016/j.molstruc.2020.129089
0022-2860/

Table 1
Optimization of reaction conditions[a].

Entry	Base (equiv.)	Solvent	Time(h)	Yield(4a)
1.	–	CH_3CN	24 h	No reaction
2.	K_2CO_3 (2)	CH_3CN	24 h	42[b]
3.	K_2CO_3 (1)	CH_3CN	24 h	32[b]
4.	K_2CO_3 (4)	CH_3CN	24 h	42[b]
5.	K_2CO_3 (4)	EtOH	24 h	42[b]
6.	K_2CO_3 (4)	THF	24 h	20[b]
7.	K_2CO_3 (4)	DCM	24 h	36[b]
8.	K_2CO_3 (4)	DMF	12 h	76
9.	K_2CO_3 (4)	DMSO	09 h	83
10.	NaOH (4)	DMSO	24 h	68
11.	Cs_2CO_3 (4)	DMSO	24 h	78
12.	K_2CO_3 (4)	DMSO	24 h	No reaction[c]

[a] **Conditions: 1a** (1.0 mmol), **2a** (1.0 mmol) and **3a** (2.0 mmol), base in 5 mL of solvent at room temperature;
[b] Incomplete Reaction;
[c] reaction was attempted under N_2 atmosphere.

Table 2
Synthesis of polyfunctionalized aminothioalkenes **(4a-4i)**.

Compound no	R^1	R^2	Ar	Time (h)	Yield (%)
4a	OMe	H	C_6H_5	09	83
4b	OMe	H	4-ClC_6H_4	08	82
4c	OMe	H	2-Naphtyl	12	85
4d	Cl	H	4-ClC_6H_4	10	85
4e	Br	H	4-BrC_6H_4	24	78
4f	Me	H	4-MeC_6H_4	12	86
4g	H	H	4-ClC_6H_4	12	81
4h	F	H	4-ClC_6H_4	24	80
4i	Cl	Cl	2-Naphthyl	12	82

ing in molecules devoid of these strong directional forces depends mainly upon weak interactions. The role of -CH group in self-assembly is well established and plays a significant role in crystal packing [44]. DFT based theoretical methods provide an alternative to crystallography for molecular structure prediction. The detailed exploration of structural features from optimized molecular geometry using DFT based methods is one of our interest [45]. [46]

Keeping in view the need of development of novel transition metal-free methodologies and continuing our interest in the same field [47–50], we have carried out metal free C–H sulfenylation of *in situ* prepared enamines and their detailed structural study using X-ray single crystal diffraction studies (XCDS) and DFT methods

2. Results and discussion

2.1. Chemistry

The direct sulfenylation of *in situ* generated enamine was investigated using a one-pot, three-component protocol, where dimethylacetylenedicarboxylate (**1a**), *p*-anisidine (**2a**) and thiophenol (**3a**) were used as model substrates. Firstly, a mixture of dimethylacetylenedicarboxylate (**1a**) (1.0 mmol) and *p*-anisidine (**2a**) (1.0 mmol) was stirred at room temperature in ethanol for 5 min. After the formation of enamine, as monitored by TLC using EtOAc: Pet ether (10:90, *v/v*) as solvent, ethanol was removed under reduced pressure and 2.0 mmol of thiophenol **(3a)** in 5 mL of CH_3CN was added to the reaction mixture. The contents were stirred at room temperature and the progress of the reaction was monitored using TLC for 24 h. No new product formation was observed in the reaction even after 24 h (Table 1, entry 1) (Scheme 1). The same model reaction was further explored using K_2CO_3 (2 equiv.) as a base. A new spot was observed on TLC, however, the reaction was incomplete even after 24 h. The reaction was quenched by adding ice. The reaction mixture was extracted using DCM, dried over anhyd. Na_2SO_4 and chromatographed over silica gel (230–400) using EtOAc: Pet ether (2:98, *v/v*) as eluent. The solid thus separated was characterized as dimethyl 2-((4-methoxyphenyl)amino)-3-(phenylthio)fumarate **(4a)** using ^{1}H NMR, ^{13}C NMR and X-ray single crystal diffraction studies (XCDS) and was obtained in 42% yield (Table 1, entry 2).

In order to develop a highly efficient and convenient methodology for the synthesis of aminothioalkenes **(4)**, the scope of the same model reaction was further explored using different concentration of base *i.e.*, 1 eq. and 4 eq. of K_2CO_3 (Table 1, entries 3 & 4). It was observed that reaction went to completion with high yield when higher concentration of base was used (Table 1, entry 4).

A variety of solvents *i.e.*, EtOH, THF, DCM, DMF and DMSO were explored in the same model reaction using K_2CO_3 (4 equiv.) as a base (Table 1, entry 5–9). In first three cases, reactions did not proceed to completion even after 24 h and gave 42%, 20% and 36% of **4a**, respectively (Table 1, entries 5–7) while in case of DMF, the reaction was complete in 12 h but gives **4a** in 76% yield (Table 1, entry 8). To our delight, the reaction carried out in DMSO at room temperature under ideal conditions resulted in 83% yield of **4a** in 9 h (Table 1, entry 9). The effect of different bases like NaOH and Cs_2CO_3 (Table 1, entries 10 & 11) was also explored. However, no significant improvement in yield and reaction time was observed in both the conditions. In order to explore the role of air, the reaction was carried out under N_2 atmosphere and no desired product **(4a)** were detected (Table 1, entry 12). It can be inferred that thiol **3a** undergoes aerobic oxidation *in situ* to disulfide. This shows that the reactions occurring *via* an aerobic oxidative cross-coupling.

It can be inferred from above results that the reaction of dimethylacetylenedicarboxylate (**1a**) (1 mmol), *p*-anisidine (**2a**) (1 mmol) and thiophenol (**3a**) (2 mmol) in presence of 4 equiv. of K_2CO_3 using DMSO as solvent is the standardized reaction condition for the synthesis of dimethyl 2-(phenyl)thio)-3-((4-methoxyphenyl)amino)fumarate **(4a)**.

The developed methodology was then extended to other substrates by carrying out reactions of dimethylacetylenedicarboxylate (**1a**) with substituted thiophenol and aniline under otherwise identical conditions (Scheme 2). All the reaction gave the corresponding polyfunctionalized alkenes in high yields in 8–24 h under similar condition **(4b-4i)**. The developed methodology failed to yield desired product when aliphatic thiol (*n*-hexanethiol) was reacted with *in situ* generated enamine under identical conditions.

We believe that the thioarylation proceeds by a nucleophilic attack of *in situ* generated enamine on diphenyldisulfide linkage followed by isomerization to give the desired product (Scheme 3). The initial formation of enamine from dialkyl acetylenedicarboxylate and aromatic amine in ethanol was followed by removal of ethanol under reduced pressure. This was followed by addition of 2 eq. of thiophenol which undergoes aerial oxidation in K_2CO_3/DMSO, followed by attack of enamine on disulphide to give the desired compound polyfunctionalized aminothioalkenes.

2.2. Molecular structure (X-ray diffraction)

The detailed molecular structure of dimethyl 2-((4-methoxyphenyl)amino)-3-(phenylthio)fumarate **(4a)** was explored using XCDS. The *trans* stereochemistry of double bond in **4a** was confirmed from the structure derived from diffraction studies (Fig. 1). The ORTEP view of the asymmetric unit along with the optimized structure of **4a** are shown in Fig. 1. The refinement details and crystallographic parameters are provided as supplementary material (Table S1). The molecule **4a** crystallises in monoclinic system within *p21/n* space group with lattice parameter a = 10.8877(2) Å, b = 20.6639(3) Å, c = 8.1934(8) Å with β= 90.502(3)° respectively.

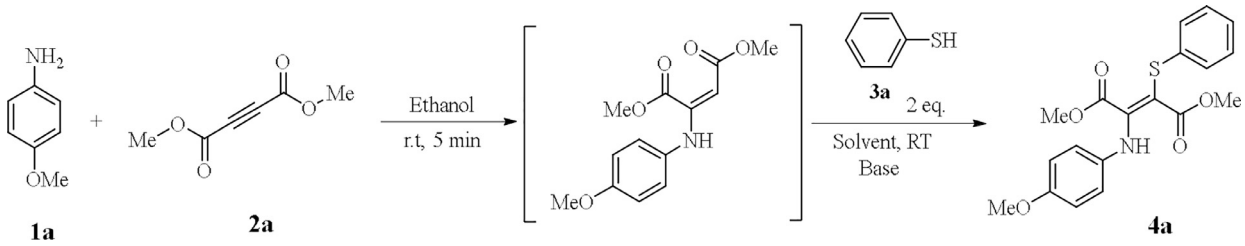

Scheme 1. Synthesis of dimethyl 2-((4-methoxyphenyl)amino)−3-(phenylthio)fumarate(**4a**).

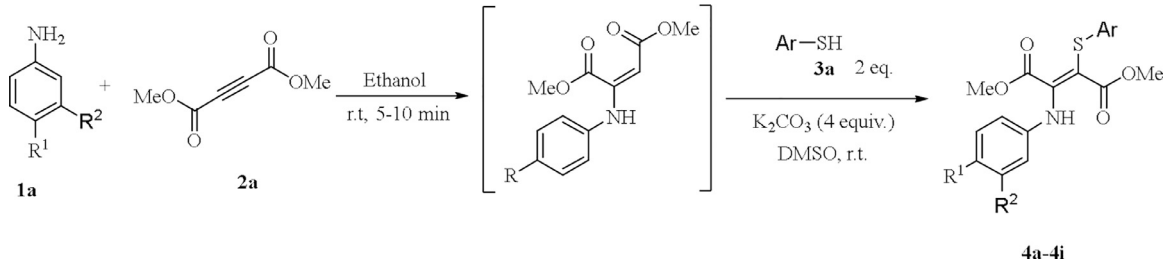

Scheme 2. One-pot synthesis of polyfunctionalized aminothioalkenes (**4a-4i**).

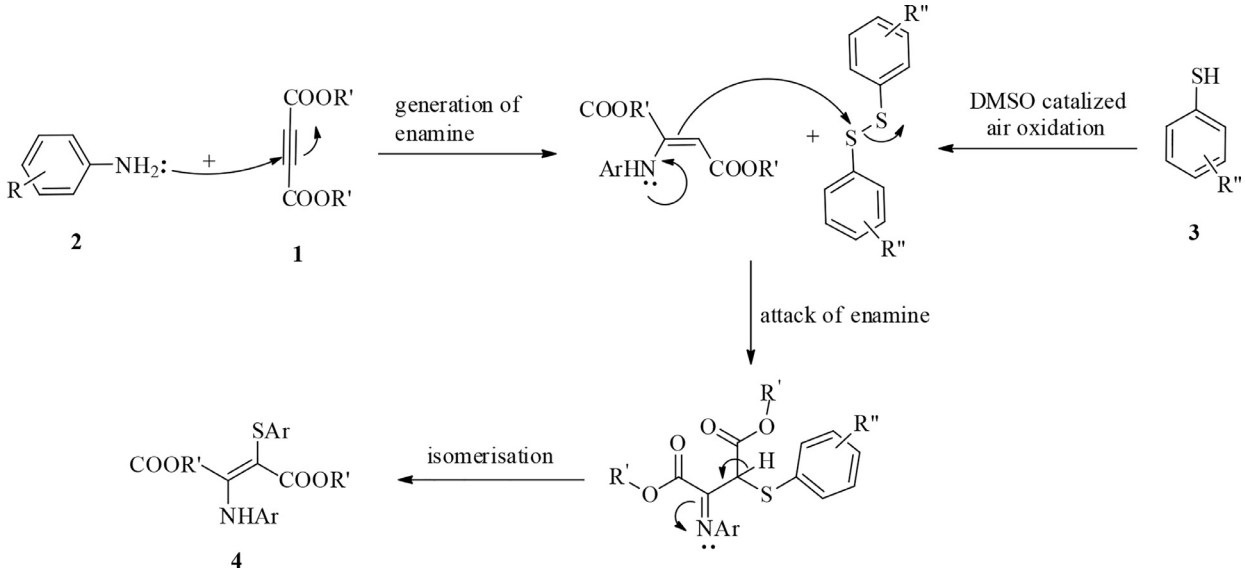

Scheme 3. Mechanism for the synthesis of polyfunctionalized aminothioalkenes (**4a-4i**).

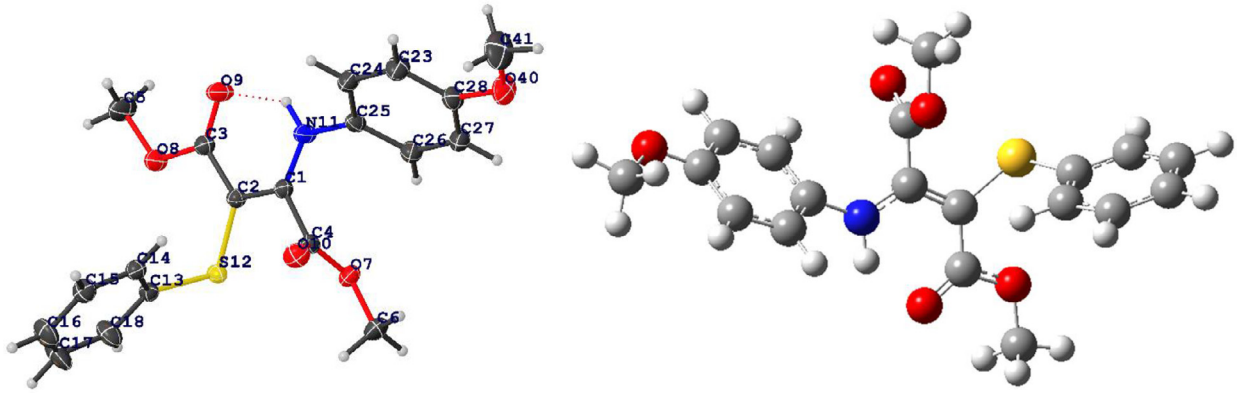

Fig. 1. **(a)** Crystal structure of dimethyl 2-((4-methoxyphenyl)amino)-3-(phenylthio)fumarate(**4a**); **(b)** Optimized geometry using DFT B3LYP/6–311+*G*(d) theory.

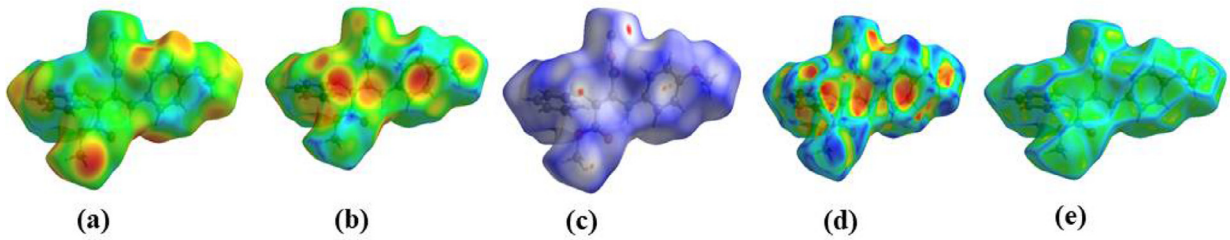

Fig. 2. Hirshfeld Surface analysis of dimethyl 2-((4-methoxyphenyl)amino)−3-(phenylthio)fumarate **(4a)** **(a)** d_i; **(b)** d_e; **(c)** d_{norm}; **(d)** Shape index; **(e)** Curvedness.

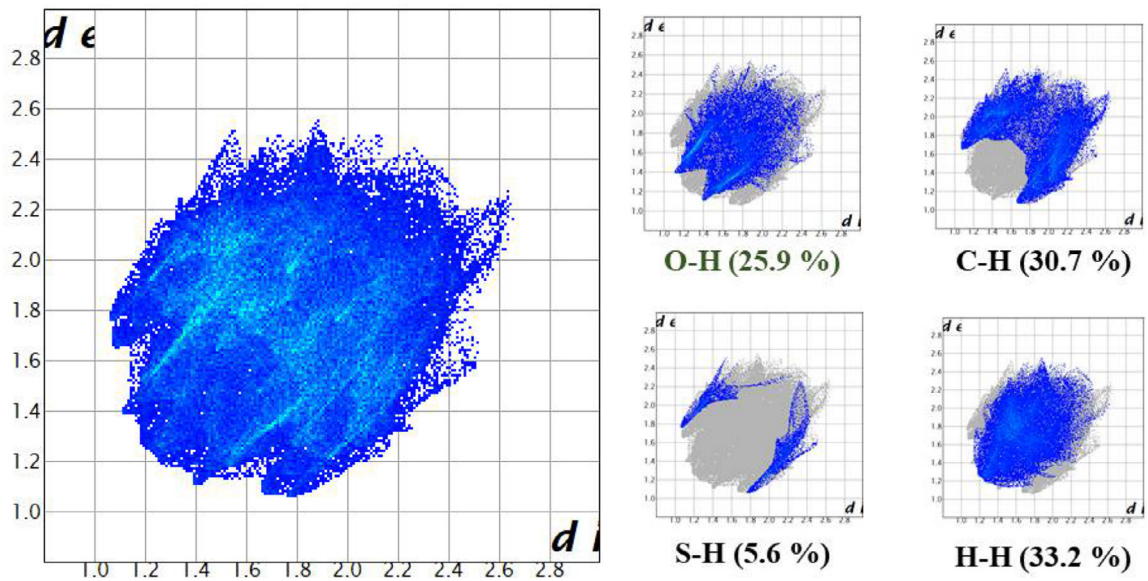

Fig. 3. 2D fingerprint regions for **4a** showing per atom intermolecular interactions.

2.3. Hirshfeld surface analysis

Structural descriptions using crystallographic techniques would be incomplete without Hirshfeld surfaces (HS) analysis as it explains different types of interactions existing within the crystals. Furthermore, HS analysis can also be used to investigate the locations and quantitative ratios of atom…atom contacts with potential weak hydrogen bond and intramolecular interactions. The HS analysis of **4a** was done using crystal explorer 17.5. HS is generally three-dimensional (3D) colored maps generated with d_{norm} using a color combination of blue, white and red. The color used in these 3D maps indicates the strength of intermolecular contacts comparable with the Van der Waals (vdW) contacts where blue color represents longer contacts, white shows vdW and red indicates shorter intermolecular contacts. The π-π stacking interactions in a molecule can be visualized with the help of a shape index tool in HS by the presence of adjacent red and blue triangles. The distance of an atom external or internal to the surface can be mapped using d_e and d_i respectively. The d_{norm} surface resulted from the normalization of d_i and d_e pair with respect to vdW radii of corresponding atoms. The HS was mapped over d_{norm} (−0.064 to 1.138 Å), d_i(1.063 to 2.548 Å), d_e(1.063 to 2.505 Å), shape index (−0.998 to 0.996 Å) and curvedness (−3.803 to 0.487 Å) to visualize the molecular structure around which these properties were calculated. HS is a practical tool for defining the surface characteristics of molecules along with the hydrogen bonding interactions and close contacts present in them. Intermolecular hydrogen bonds are the close contacts represented by deep-red large circular spots visible on HS mapped over d_{norm}, whereas, contacts weaker than hydrogen bonding are represented by diminutive spots on the surface (Fig. 2).

The summary of intermolecular contacts in the crystal structures was extracted from crystallographic data by generating 2D fingerprint plots by a combination of *d*e and *d*i and binding them into intervals of 0.01 Å. The HS was decomposed further into fingerprint plots, which defines all significant intermolecular interactions and their contribution to HS. The H–H type of interaction contributes 57.2% of the total HS. However, the contribution made by hydrogen bonding interactions in the form of O–H and S-H is 25.9% and 5.6% of the total interaction respectively. The C–H type of interaction contributes 30.7% in the total Hirshfeld surface and represented by outermost spikes present in the fingerprint plot (Fig. 3).

2.4. Molecular self-assembly

Various inter and intramolecular interactions present in the case of **4a** are calculated using PARST [51]. The presence of eight potential hydrogen bond donor –CH groups establish C—H•••O as the most significant intermolecular interactions in case of **4a**. The molecules of **4a** form dimers associated with a crystallographic glide plane (Fig. 4) and linked through moderate O_{10}…H_{26} (2.705 Å) and C_{14}…H_{6C} (2.773 Å) hydrogen bond. Due to the absence of strong -OH and -NH based hydrogen bond donor, the **4a** assembled mainly through C–H interactions. The main D-H—A type interactions present in **4a** along with close contacts are tabulated in Table 3.

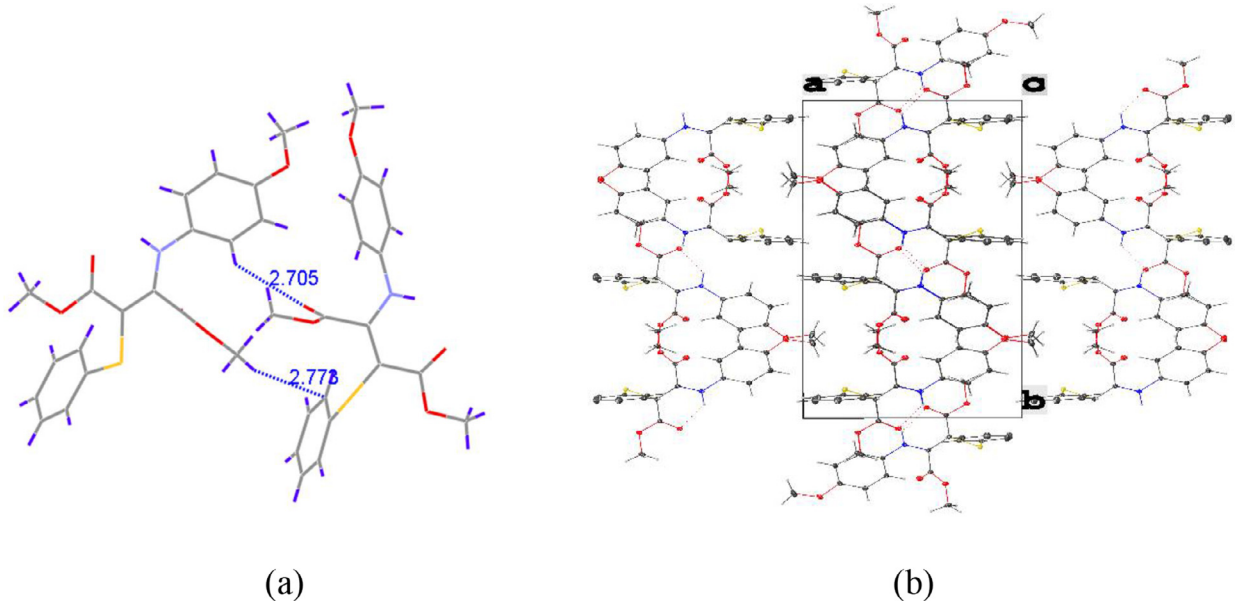

Fig. 4. **(a)** Dimer of **4a** associated with a crystallographic glide plane; (b) Crystal packing along *ab* plane.

Table 3
Potential non-covalent interactions present in case of **4a** [Å and °].

D-H–A type interactions*				
D-H–A	d(D-H)	d(H–A)	d(D–A)	<(DHA)
N_{11}–H_{11}–O_9*	1.030	2.659	1.893	128.55
C_{26}–H_{26}–O_7*	1.080	3.205	2.496	122.28
C_6–H_{6A}-O_{10}*	1.080	2.651	2.604	80.60
C_6–H_{6B}-O_{10}*	1.080	2.651	2.660	77.81
C_5–H_{5B}-O_9*	1.080	2.607	2.590	78.89
C_5–H_{5c}-O_9*	1.080	2.607	2.576	79.62
C_{14}–H_{14}–O_9#1	1.080	3.206	2.508	121.39
C_5–H_{5B}-O_{10}#1	1.080	3.849	2.773	173.76
C_{15}–H_{15}–O_9#1	1.080	3.286	2.680	115.05
C_6–H_{6c}-O_{10}#2	1.080	3.120	2.859	93.67
C_{27}–H_{27}–O_{10}#2	1.080	3.377	2.730	118.23
C_{26}–H_{26}–O_{10}#2	1.080	3.328	2.622	122.46
C_6–H_{6B}-O_{10}#2	1.080	3.120	2.735	100.64
C_{18}–H_{18}–O_8#3	1.080	3.499	2.707	129.90
C_{41}–H_{41c}-O_{40}#4	1.080	3.864	2.873	152.56
C_6–H_{6A}-O_7#4	1.080	3.728	2.798	144.21
C_{16}–H_{16}-S_{12}#5	1.080	3.820	2.831	152.25
C_5–H_{5A}-O_{40}#6	1.080	3.668	2.712	147.32
Close contacts				
Interaction	Distance (Å)	Interaction	Distance (Å)	
O_9…H_{14}#1	2.589	O_{10}…H_{27}#4	2.8037	
H_{26}…H_{6B}#2	2.5931	O_8…H_{18}#3	2.8056	
H_{11}…H_{15}#1	2.6825	H_{14}…H_{6C}#4	2.859	
O_{10}…H_{26}#4	2.7051	O_{10}…H_{6C}#4	2.8694	
O_{10}…H_{6B}#4	2.7596	H_{41A}…H_{41C}#4	2.8718	
C_{14}…H_{6C}#4	2.7727	H_{41C}…H_{41A}#4	2.8718	

Values normalized following R.Taylor et al. [52].
* intramolecular interactions; Symmetry transformations used to generate equivalent atoms: **#1** -*x* + 1,-y,-*z*; **#2** x,-*y* + 1/2,+*z* + 1/2; **#3** -x,-y,-*z*; **#4** x,-*y* + 1/2,+*z*-1/2; **#5** x,+*y*,+*z*-1; **#6** -*x* + 1,+*y*-1/2,-*z* + 1/2.

2.5. DFT based conformational studies

In order to explore the most stable conformation of **4a,** potential energy scan (PES) was applied along dihedral angle N_{11}–C_1–C_2–C_3 (Fig. 5). It has been revealed from PES that the *trans* form of **4a** is 2.3 kcal/mol more stabilized than the *cis* form. The extra stabilization in case of *trans* over *cis* form was attributed due to the presence of steric hindrance in later case. The geometry of both *cis* and *trans* form were optimized using the same DFT method. The sum of electronic and zero-point energy for *cis* and

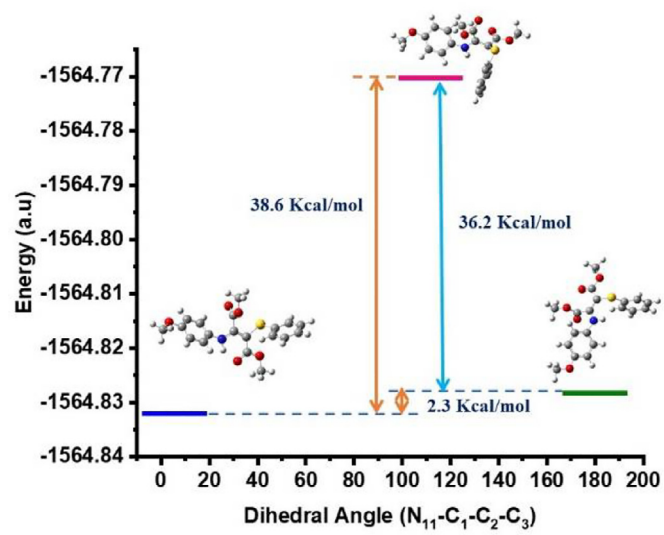

Fig. 5. Potential energy scan applied along dihedral angle N_{11}–C_1–C_2–$C_3$for **4a**.

trans form is −1564.478472 a.u and −1564.481937 a.u respectively. The results of DFT based optimization suggest that *trans* form of **4a** is more stable than its *cis* form which are in line with the results obtained from x-ray single crystallography.

3. Electrostatic results

3.1. Global reactivity descriptors

The geometries of polyfunctionalized aminothioalkenes **(4a-4i)** were optimized using DFT method with B3LYP/6–311+*G*(d) level of theory and frontier molecular orbitals (FMO's) were computed. According to FMO theory the stability, reactivity, electronic transitions and intermolecular interactions of a compound are contained within well known quantum chemical parameters *i.e.*, HOMO and LUMO [53–55]. These orbitals signify that the electron accepting and donating behavior of a molecule can be utilized for ciphering the reactivity of π-electron framework in conjugated systems [56]. The distribution of FMO's in a molecule decides the biological re-

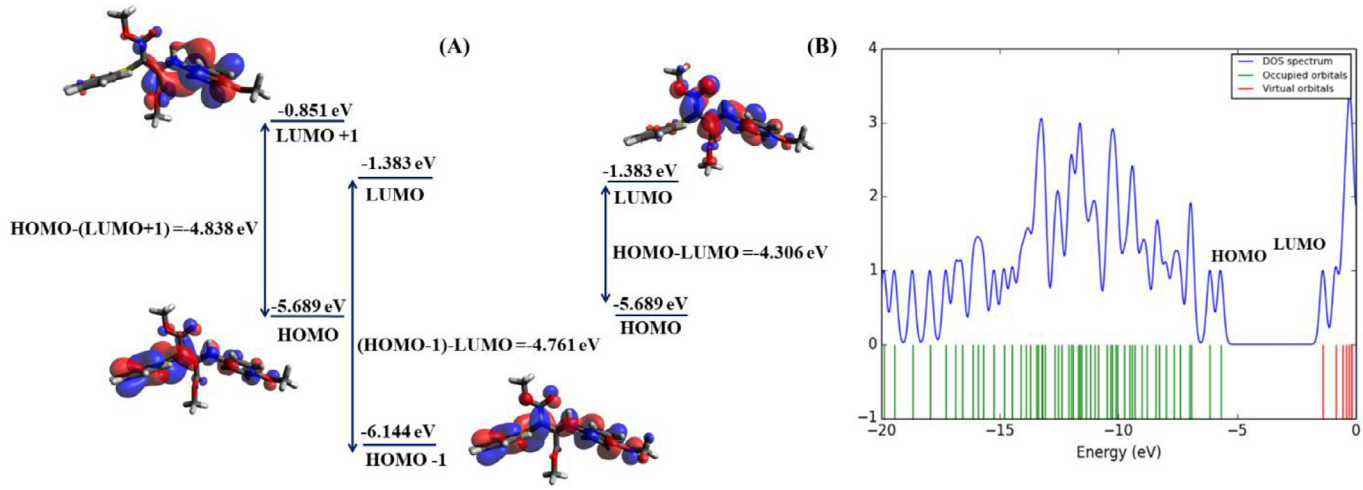

Fig. 6. Pictorial representation of **(A)** HOMO-LUMO**; (B)** Density of states for **4a**.

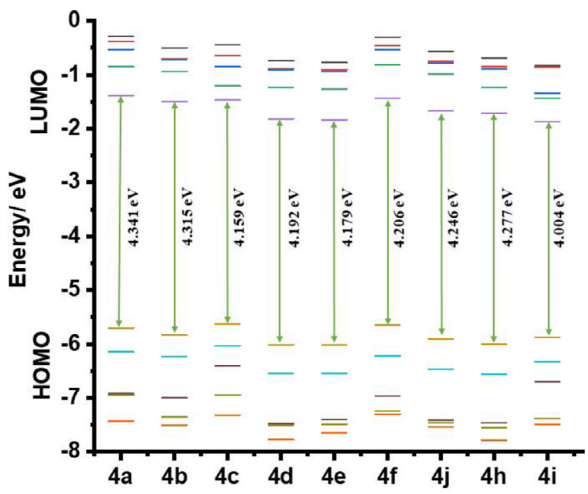

Fig. 7. FMO of polyfunctionalized aminothioalkenes **(4a-4i)** and their energy gap.

sponse associated with it, their presence on the same side strongly reduces the biological activity. The distribution pattern of FMO's along with density of states (DOS) for **4a** is shown in Fig. 6.

The green and red lines represent the energy levels for occupied and empty orbitals respectively. It has been revealed that π-electron cloud of HOMO is mainly distributed over phenyl ring attached to sulfur, however, the LUMO is mainly concentrated over ester and phenyl ring attached with the nitrogen atom. The energy difference between these FMO's for polyfunctionalized aminothioalkenes is shown in Fig. 7.

The chemical reactivity descriptors includes chemical potential (μ), chemical Hardness (η), electrophilicity index (ω), Fukui function (Δf) and Nucleophilicity index (N) which provide a deep insight into the chemical reactivity and stability of polyfunctionalised aminothioalkenes [57,58,59]. The properties associated with these descriptors are further categorised into global and local reactivity descriptors. Hardness is one of the important terms which relate to the biological activity of a compound. The molecules associated with a large HOMO-LUMO energy gap are comparatively harder and more stable than the molecules with a small gap. The chemical potential (μ) describes the intramolecular charge transfer phenomenon in the ground state and the tendency of electrons to escape from the equilibrium state. Hence, chemically reactive molecules are associated with large values of chemical potential. The energy change associated with the flow of electrons from HOMO to LUMO is defined mathematically by electrophilicity index (ω). The energy of HOMO and LUMO along with global reactivity descriptors calculated for all the polyfunctionalised aminothioalkenes **(4a-4i)** are summarized in Table 4.

The local reactivity of a molecule can be defined in terms of local reactivity descriptors *i.e.,* Fukui function, which can be defined as the distortion of electron density upon accepting and donating electrons in particular nuclei. Fukui functions in its condensed form is the most practical way to investigate the ability of an atom to serve as a reactive site in the molecule. The nucleophilic, electrophilic and radical sites in a molecule can be expressed using Fukui functions in its condensed form by f_x^-, f_x^+ and f_x^0 as respectively. Following expressions are used to access these condensed Fukui function

$$f_x^- = q^N - q^A;\ f_x^+ = q^C - q^N \text{ and } f_x^0 = \left(q^C - q^A\right)/2$$

The electronic population in neutral, cationic and anionic species can be represented by q^N, q^C and q^A. The charge present on each atom in neutral, positive and negative state of the molecule was accessed using natural charge derived from NBO analysis. Morrel *et al.* had proposed a new dual descriptor $\Delta f(r)$ for differentiating reactive sites within a molecule, where electrophilic sites are associated with positive $\Delta f(r)$ and nucleophilic sites are with negative $\Delta f(r)$ values. [60] The results calculated for **4a** are summarized in Table S2. The new dual descriptor is defined by following equation.

$$\Delta f(r) = f_x^+ - f_x^-$$

3.2. Molecular electrostatic potential (MEP)

The reactive and hydrogen bonding sites along with electron density can be significantly recognised visually using MEP and can be used for the evaluation of reactive sites in a molecule [61]. Furthermore, the electronegativity and dipole moment are some of the significant properties that can be predicted using DFT based MEP calculations. The electrostatic potential over the surface of the molecule was mapped using different color combinations. The region of zero, positive and negative potential are represented using white, red and blue color respectively (Fig. 8.) It can be seen from MEP plot that the negative electrostatic potential was spread over carbonyl oxygen atom and sulfur indicating possible electrophilic sites while electropositive region is mainly distributed over nitrogen atom attached to double bond. The presence of positive charge

Table 4
Electrostatic properties of polyfunctionalized aminothioalkenes **(4a-4i)**.

S.No	HOMO	LUMO	Chemical potential (μ)= $(I + A)/2$	Chemical hardness (η)= (I-A)/2[a]	Electrophilicty Index (ω)= $\mu^2/2\eta$	Nucleophilicity index (N)[b]
4e	−6.011	−1.832	−3.921	2.090	3.679	3.477
4d	−6.008	−1.816	−3.912	2.096	3.65	3.48
4i	−5.875	−1.871	−3.873	2.002	3.747	3.613
4h	−5.993	−1.716	−3.854	2.138	3.474	3.495
4 g	−5.907	−1.661	−3.784	2.123	3.373	3.581
4b	−5.833	−1.492	−3.662	2.17	3.09	3.655
4c	−5.628	−1.469	−3.549	2.079	3.028	3.86
4a	−5.698	−1.383	−3.541	2.158	2.906	3.79
4f	−5.644	−1.438	−3.541	2.103	2.981	3.844

[a] I= -E_{HOMO}, A= -E_{LUMO}.
[b] Calculated using N = E_{HOMO} (Compound)-E_{HOMO}(Tetracyanoethylene) [59].

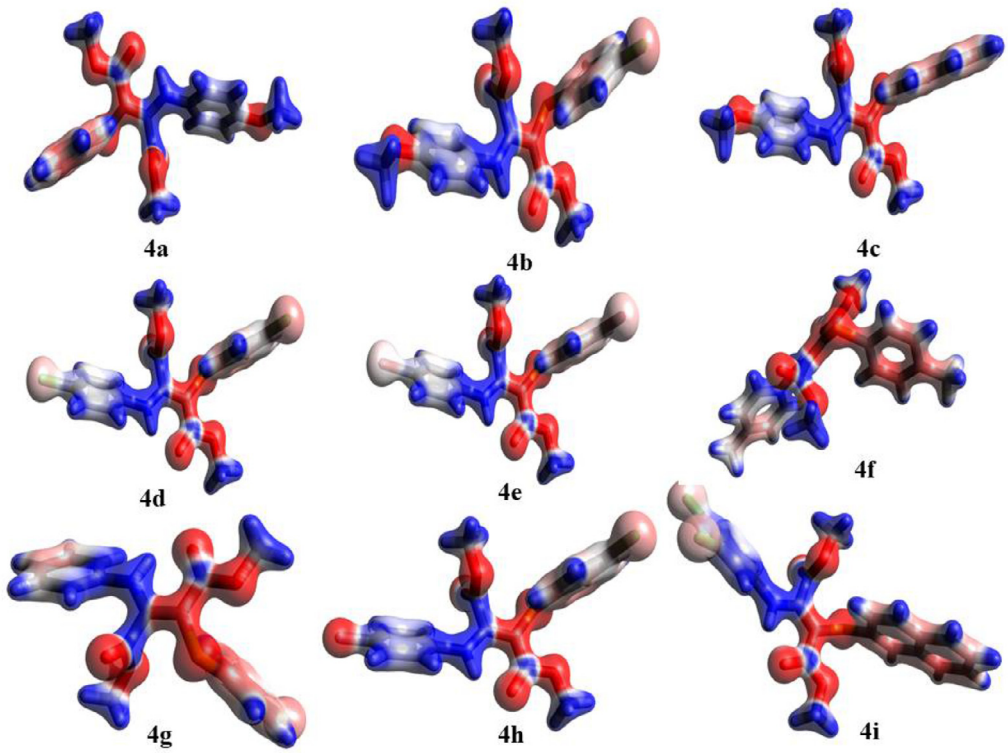

Fig. 8. ESP surface mapped over electron density for polyfunctionalized aminothioalkenes **(4a-4i).**

on H_{36} and negative on O_9 indicates the probability of intramolecular hydrogen bonding between them. The findings of MEP plot supports the presence of intramolecular hydrogen bonding in the crystal structure of **4a**. Moreover, the contribution of O–H interaction is 25.9% of the overall interactions present in the crystal structure quantified using 2D fingerprint.

3.3. NBO & NLO analysis (DFT based)

The different properties like stability, basicity, reactivity, intermolecular charge transfer, the relationship between donor and acceptor associated with a molecule can be explored in an efficient way by Natural Bond orbital (NBO) analysis [62]. Second order perturbation theory explains the nature of non-Lewis acceptors and Lewis donor, and can be used to explore hyperconjugative interaction energies. The intensity of hyperconjugative interactions can be ascertained using E(2) value. The intensive interactions are associated with a large E(2) values, and the intense values of E(2) present in case of **4a** are given in Table S3.

Development of non-linear optical material attracts scientific community as these materials can be used in various applications like optical modulation, telecommunication, signal processing, optical memories and optical interconnections [63]. The dipole moment of the system rearranges upon exposure to an external electric field, where linear and non-linear optical behavior of the molecule can be predicted using polarizability (α) and hyperpolarizibility (β) values. The NLO properties related to a molecule can be predicted in an inexpensive way by DFT based calculations. First hyperpolarizability (β_0) of a molecule is the basis of NLO properties and urea is used as a prototype for comparative studies. The hyperpolarizability tensors (β_{xxx}, β_{xxy}, β_{xyy}, β_{yyy}, β_{xxz}, β_{xyz}, β_{yyz}, β_{xzz}, β_{yzz}, β_{zzz}) of **4a** were obtained from Gaussian log file as calculated using DFT method (Table S4). The hyperpolarizability (β) values obtained in atomic units have been converted into electronic units (e.s.u) (β; 1 a.u.= 8.6393 × 10^{-33}esu). The value of first order hyperpolarizibility (β_0) calculated for all the compounds is listed in Table 5. The β_0 of **4b** is 2.03 × 10^{-30} e.s.u is 17 times greater than urea 0.12 × 10^{-30} e.s.u and is listed in Table 5.

$$\beta_0 = \left[(\beta_{xxx}+\beta_{xyy}+\beta_{xzz})^2+(\beta_{yyy}+\beta_{xzz}+\beta_{yxx})^2+(\beta_{zzz}+\beta_{zxx}+\beta_{zyy})^2\right]^{1/2}$$

Table 5
Non-linear optical properties of polyfunctionalised aminothioalkenes (**4a-4j**).

Compounds	4a	4b	4c	4d	4e	4f	4 g	4h	4i	Urea
β_0 (e.s.u) x 10^{-30}	1.27	2.03	1.75	0.81	0.89	0.35	0.97	0.72	1.48	0.12

4. Conclusion

A transition metal-free protocol has been developed for the synthesis of novel polyfunctionalized aminothioalkenes *via* direct C–H sulfenylation of *in situ* generated enamines. The reaction was performed using a catalytic amount of inexpensive and nontoxic K_2CO_3 under mild reaction conditions. All the reactions resulted in good to excellent yields. The cross-coupling reaction has been achieved by aerobic oxidation without any additional oxidant at room temperature with good functional group tolerance. We believe that this is one of the simplest methodologies that provide a straightforward approach for thiolation. The molecular architecture and stereochemistry has been established using X-ray single crystal diffraction and DFT based studies. Hirshfeld surface analysis has been used to explore the intramolecular and intermolecular interactions present in the case of **4a**. Moreover, the intramolecular hyperconjugative interactions have been investigated using natural bond orbitals (NBOs) analysis and their intensity was categorized according to their second order stabilization energy (E(2)). The electrostatic properties such as global reactivity descriptors, local reactivity descriptors, ESP and NLO have been investigated using DFT method and B3LYP/6–311+*G*(d) level of theory. Crystal data reveals strong intramolecular hydrogen bond in the molecule and DFT studies suggest that these molecules can be explored as potential candidates in excited state proton transfer phenomenon.

5 Experimental

5.1 Chemistry

All the chemicals, solvents and reagents are commercial and procured from Sigma-Aldrich, Merck and Spectrochem and were used as received. The Progress of the reaction was monitored by thin layer chromatography by using Pre-coated thin layer aluminum sheets (GF-254). The ^{1}H NMR and proton decoupled ^{13}C spectra were recorded on JEOL JNM ECX-400 P at 400 and 100 MHz respectively, using TMS as an internal standard. The chemical shifts values are recorded on δ scale and the coupling constants (*J*) are in Hz.

5.1.1 Typical procedure for the synthesis of polyfunctionalized aminothioalkenes (4a-4i)

A mixture of dimethylacetylenedicarboxylate (**1**) (1.0 mmol), aromatic amine (**2a**) (1.0 mmol) in 5 mL of EtOH was added to a 50 mL round-bottomed flask mounted over a magnetic stirrer. The reaction was monitored by TLC using EtOAc: Pet ether (10:90, *v/v*) as eluent. After the disappearance of reactant in the reaction mixture, the solvent was removed under reduced pressure and 2 equiv. of thiophenol **(3a)** was added to the reaction mixture in 5 mL of DMSO. The mixture was stirred at room temperature. The reaction was monitored by TLC using EtOAc: Pet ether (20:80, *v/v*) as eluent. After completion of the reaction, 50 mL of water was added to the reaction mixture. The reaction mixture was extracted using DCM (2 × 10 mL), dried over anhyd. Na_2SO_4 and chromatographed over silica gel (230–400) using EtOAc: Pet ether (2:98, *v/v*) as eluent. to afford pure polyfunctionalized aminothioalkenes **(4a-4i)**. Various spectral techniques like ^{1}H NMR and ^{13}C NMR were used for the characterization of compound.

5.1.2 Spectral data

Dimethyl 2-((4-methoxyphenyl)amino)-3-(phenylthio)fumarate (4a)
Off white solid; ^{1}H NMR (400 MHz, $CDCl_3$)δ_H 10.73 (s, 1H, NH), 7.25 (d, *J* = 3.2 Hz, 4H, ArH), 7.20–7.05 (m, 3H, ArH), 6.84 (d, *J* = 9.2 Hz, 2H, ArH), 3.79 (s, 3H, $COOCH_3$), 3.71 (s, 3H, $COOCH_3$), 3.64–3.57 (s, 3H, $ArOCH_3$); ^{13}C NMR (100 MHz, $CDCl_3$)δ_C 170.60, 162.94, 159.90, 158.09, 138.63, 130.99, 128.55, 126.12, 125.26, 125.11, 114.40, 84.30, 55.37, 52.39, 52.03.

Dimethyl 2-((4-chlorophenyl)thio)-3-((4-methoxyphenyl)amino)fumarate (4b)
Off white solid; ^{1}H NMR (400 MHz, $CDCl_3$)δ_H 10.73 (s, 1H, NH), 7.20 (m, 4H, ArH), 7.11 (d, *J* = 8.7 Hz, 2H, ArH), 6.85 (d, *J* = 9.2 Hz, 2H, ArH), 3.80 (s, 3H, $COOCH_3$), 3.71 (s, 3H, $COOCH_3$), 3.60 (s, 3H, $ArOCH_3$); ^{13}C NMR (100 MHz, $CDCl_3$)δ_C 170.42, 162.88, 160.11, 158.23, 137.34, 131.13, 130.86, 128.71, 127.47, 125.21, 114.45, 83.87, 55.41, 52.50, 52.12.

Dimethyl 2-((4-methoxyphenyl)amino)-3-(naphthalen-2-ylthio)fumarate(4c)
Off white solid; ^{1}H NMR (400 MHz, $CDCl_3$)δ_H 10.80 (s, 1H, NH), 7.75 (m, 3H, ArH), 7.67 (d, *J* = 8.2 Hz, 1H, ArH), 7.41 (m, 3H, ArH), 7.14 (d, *J* = 8.7 Hz, 2H, ArH), 6.85 (d, *J* = 8.2 Hz, 2H, ArH), 3.79 (s, 3H, $COOCH_3$), 3.69 (s, 3H, $COOCH_3$), 3.59 (s, 3H, $ArOCH_3$); ^{13}C NMR (100 MHz, $CDCl_3$) δ_C 170.69, 162.98, 158.15, 136.25, 133.69, 131.61, 131.02, 128.16, 127.68, 127.11, 126.27, 125.14, 124.66, 123.89, 114.45, 84.17, 55.41, 52.47, 52.12.

Dimethyl 2-((4-chlorophenyl)amino)-3-((4-chlorophenyl)thio)fumarate (4d)
Off white solid; ^{1}H NMR (400 MHz, $CDCl_3$)δ_H 10.88 (s, 1H, NH), 7.30 (d, *J* = 8.7 Hz, 2H, ArH), 7.21 (m, 4H, ArH), 7.14–7.04 (m, 2H, ArH), 3.72 (s, 3H, $COOCH_3$), 3.67 (s, 3H, $COOCH_3$); ^{13}C NMR (100 MHz, $CDCl_3$)δ_C 170.28, 162.79, 158.45, 136.71, 131.89, 131.43, 129.59, 128.80, 124.81, 123.91, 86.53, 52.73, 52.30.

Dimethyl 2-((4-bromophenyl)amino)-3-((4-bromophenyl)thio)fumarate (4e)
Off white solid; ^{1}H NMR (400 MHz, $CDCl_3$)δ_H 10.89 (s, 1H, NH), 7.45 (d, *J* = 6.9 Hz, 2H, ArH), 7.37 (d, *J* = 8.7 Hz, 2H, ArH), 7.12 (d, *J* = 8.2 Hz, 2H, ArH), 7.02 (d, *J* = 8.7 Hz, 2H, ArH), 3.72 (s, 3H, $COOCH_3$), 3.67 (s, 3H, $COOCH_3$); ^{13}CNMR (100 MHz, $CDCl_3$)δ_C 170.25, 162.77, 158.33, 137.48, 137.20, 132.57, 131.70, 127.96, 124.09, 119.62, 119.28, 84.45, 52.78, 52.34.

*Dimethyl 2-(*p*-tolylamino)-3-(*p*-tolylthio)fumarate (4f)*
Off white solid; ^{1}H NMR (400 MHz, $CDCl_3$)δ_H 10.81 (s, 1H, NH), 7.18 (d, *J* = 8.2 Hz, 2H, ArH), 7.12 (d, *J* = 8.2 Hz, 2H, ArH), 7.05 (m, 4H, ArH), 3.71 (s, 3H, $COOCH_3$), 3.66 (s, 3H, $COOCH_3$), 2.31 (s, 6H, $2xArCH_3$); ^{13}C NMR (100 MHz, $CDCl_3$)δ_C 170.66, 163.14, 158.89, 136.05, 135.68, 135.24, 134.90, 129.94, 129.40, 126.66, 122.65, 85.79, 52.46, 52.09, 20.95, 20.89.

Dimethyl 2-((4-chlorophenyl)thio)-3-(phenylamino)fumarate (4 g)
Off white solid; ^{1}H NMR (400 MHz, $CDCl_3$)δ_H 10.94 (s, 1H, NH), 7.33 (t, *J* = 8.0 Hz, 2H, ArH), 7.25–7.18 (m, 5H, ArH), 7.17–7.12 (m, 2H, ArH), 3.72 (s, 3H, $COOCH_3$), 3.65 (s, 3H, $COOCH_3$); ^{13}C NMR (100 MHz, $CDCl_3$)δ_C 170.34, 162.95, 158.89, 138.10, 137.13, 131.27, 129.46, 128.75, 127.64, 126.32, 122.58, 85.54, 52.57, 52.20.

Dimethyl 2-((4-chlorophenyl)thio)-3-((4-fluorophenyl)amino)fumarate (4 h)

Off white solid; ^{1}H NMR (400 MHz, $CDCl_3$)δ_H 10.79 (s, 1H, NH), 7.27–7.12 (m, 6H, ArH), 7.03 (t, J = 8.5 Hz, 2H, ArH), 3.72 (s, 3H, $COOCH_3$), 3.63 (s, 3H, $COOCH_3$); ^{13}C NMR (100 MHz, $CDCl_3$)δ_C 170.34, 162.74, 161.03(d, $^1J_{C\text{-}F}$ = 246 Hz), 159.39, 137.01, 134.14, 131.38, 128.77, 127.72, 125.33, 116.26 (d, $^2J_{C\text{-}F}$ = 24.7 Hz), 85.57, 52.54, 52.15.

Dimethyl 2-((3,4-dichlorophenyl)amino)-3-(naphthalen-2-ylthio)fumarate(4i)

Off white solid; ^{1}H NMR (400 MHz, $CDCl_3$)δ_H 10.95 (s, 1H, NH), 7.81–7.72 (m, 3H, ArH), 7.66 (s, 1H, ArH), 7.49–7.35 (m, 4H, ArH), 7.29 (d, J = 2.7 Hz, 1H, ArH), 7.02 (dd, J = 8.7, 2.7 Hz, 1H, ArH), 3.71 (s, 6H, 2 X $COOCH_3$); ^{13}C NMR (100 MHz, $CDCl_3$)δ_C 170.65, 163.05, 158.27, 137.49, 135.77, 133.82, 132.68, 131.82, 128.41, 127.83, 127.26, 126.50, 125.46, 124.91, 124.41, 124.12, 119.56, 87.16, 52.87, 52.45.

5.2 X-ray crystal studies

The single crystal of compound **4a** suitable for X-ray analysis was obtained by slow evaporation method using acetonitrile as solvent. Single, clear, whitish block of single crystal of **4a** suitable for X-ray was mounted on Xcalibur, Sapphire3 diffractometer using mylar loop. The data collection was done at a steady temperature of T = 298 K. The structure was solved using Olex2 [64] and the model was refined with ShelXL using full matrix least squares minimisation on F^2 [65]. The final completeness is 100% out to 29.556° in Θ. A multi-scan absorption correction was performed using CrysAlisPro 1.171.38.46 (Rigaku Oxford Diffraction, 2015) Empirical absorption correction using spherical harmonics, implemented in SCALE3 ABSPACK scaling algorithm. The absorption coefficient μ of this material is 0.205 mm^{-1} at this wavelength (λ = 0.71073 Å) and the minimum and maximum transmissions are 0.796 and 1.000. Crystal explorer 17.5 was used for Hirshfeld surface generation and 2d fingerprint analysis [66]. Crystallography data excluding structure factors has been deposited on Cambridge crystallography database with CCDC no. **1,993,445** for **4a**.

5.3 Computational details of dft studies

All DFT calculations presented in the present manuscript were performed with Gaussian 09 program package [67] using hybrid exchange correlation functional B3LYP and 6–311(+)G(d) basis set [68]. Initially, the geometry of all the polyfunctionalized aminothiols **(4a-4i)** was optimized using same level of theory. No imaginary frequencies were found for any of the structure, which indicates their stability at global minima. Density of states (DOS) were calculated using Gausssum 3.0. [69] After optimization of the molecular geometries, the global reactivity descriptors were calculated utilizing the information contained in FMO's [70,71]. The NBO calculations were performed using NBO 3.0 program implemented in Gaussian 09 W package using the same level of theory to explore the hyperconjugative interaction present in the molecule [72]. Thereafter, Fukui function were calculated from same NBO analysis at same level of theory to explore the possibility of charge transfer in polyfunctionalized aminothiols **(4a-4i)**. Avogardo 2.0 was used for the visualization of the results of DFT calculations. [73]

Declaration of Competing Interest

The authors declare that they have no known competing financial interests or personal relationships that could have appeared to influence the work reported in this paper.

Acknowledgement

The authors thanks SAIF, PU for spectral data

Supplementary materials

Supplementary material associated with this article can be found, in the online version, at doi:10.1016/j.molstruc.2020.129089.

References

[1] I.P. Beletskaya, V.P. Ananikov, Transition-metal-catalyzed C-S, C-Se, and C-te bond formation via cross-coupling and atom-economic addition reactions, Chem. Rev 111 (2011) 1596–1636, doi:10.1021/cr100347k.
[2] G. La Regina, A. Coluccia, A. Brancale, F. Piscitelli, V. Gatti, G. Maga, A. Samuele, C. Pannecouque, D. Schols, J. Balzarini, Indolylarylsulfones as HIV-1 non-nucleoside reverse transcriptase inhibitors: new cyclic substituents at indole-2-carboxamide, J. Med. Chem. 54 (2011) 1587–1598.
[3] T. Punniyamurthy, S. Velusamy, J. Iqbal, Recent advances in transition metal catalyzed oxidation of organic substrates with molecular oxygen, Chem. Rev 105 (2005) 2329–2364.
[4] M. Klečka, R. Pohl, J. Čejka, M. Hocek, Direct C–H sulfenylation of purines and deazapurines, Org. Bimol. Chem 11 (2013) 5189–5193.
[5] I.M. Yonova, C.A. Osborne, N.S. Morrissette, E.R. Jarvo, Diaryl and heteroaryl sulfides: synthesis via sulfenyl chlorides and evaluation as selective anti-breast-cancer agents, J. Org. Chem. 79 (2014) 1947–1953.
[6] T. Kondo, T. Mitsudo, Metal-catalyzed carbon− sulfur bond formation, Chem. Rev 100 (2000) 3205–3220.
[7] S. Tang, K. Liu, C. Liu, A. Lei, Olefinic C–H functionalization through radical alkenylation, Chem. Soc. Rev 44 (2015) 1070–1082.
[8] S.I. Kozhushkov, L. Ackermann, Ruthenium-catalyzed direct oxidative alkenylation of arenes through twofold C–H bond functionalization, Chem. Sci 4 (2013) 886–896.
[9] D.-.H. Wang, K.M. Engle, B.-.F. Shi, J.-.Q. Yu, Ligand-enabled reactivity and selectivity in a synthetically versatile aryl C–H olefination, Science (80-.). 327 (2010) 315–319.
[10] A.B. Dounay, L.E. Overman, The asymmetric intramolecular Heck reaction in natural product total synthesis, Chem. Rev 103 (2003) 2945–2964.
[11] D. Mc Cartney, P.J. Guiry, The asymmetric Heck and related reactions, Chem. Soc. Rev 40 (2011) 5122–5150.
[12] G. Dyker, Handbook of CH transformations: applications in organic synthesis, Wiley-VCH, 2005.
[13] T.W. Lyons, M.S. Sanford, Palladium-catalyzed ligand-directed C− H functionalization reactions, Chem. Rev 110 (2010) 1147–1169.
[14] D.A. Colby, R.G. Bergman, J.A. Ellman, Rhodium-catalyzed C− C bond formation via heteroatom-directed C− H bond activation, Chem. Rev 110 (2009) 624–655.
[15] X. Chen, K.M. Engle, D. Wang, J. Yu, Palladium (II)-catalyzed C-H activation/C-C cross-coupling reactions: versatility and practicality, Angew. Chem 48 (2009) 5094–5115.
[16] J. Wencel-Delord, T. Droege, F. Liu, F. Glorius, Towards mild metal-catalyzed C–H bond activation, Chem. Soc. Rev 40 (2011) 4740–4761.
[17] S.H. Cho, J.Y. Kim, J. Kwak, S. Chang, Recent advances in the transition metal-catalyzed twofold oxidative C–H bond activation strategy for C–C and C–N bond formation, Chem. Soc. Rev 40 (2011) 5068–5083.
[18] C.-.L. Sun, B.-.J. Li, Z.-.J. Shi, Direct C− H transformation via iron catalysis, Chem. Rev 111 (2010) 1293–1314.
[19] L. Ackermann, Carboxylate-assisted transition-metal-catalyzed C− H bond functionalizations: mechanism and scope, Chem. Rev 111 (2011) 1315–1345.
[20] B.M. Trost, Atom economy—A challenge for organic synthesis: homogeneous catalysis leads the way, Angew. Chem 34 (1995) 259–281.
[21] B.M. Trost, The atom economy–a search for synthetic efficiency, Science (80-.). 254 (1991) 1471–1477.
[22] N. Winterton, Twelve more principles of green chemistry, Green Chem 3 (2001) G73–G75.
[23] F. Yang, S. Tian, Iodine-Catalyzed Regioselective Sulfenylation of Indoles with Sulfonyl Hydrazides, Angew. Chem 52 (2013) 4929–4932.
[24] X. Zhao, L. Zhang, T. Li, G. Liu, H. Wang, K. Lu, P-Toluenesulphonic acid-promoted, I2-catalysed sulphenylation of pyrazolones with aryl sulphonyl hydrazides, Chem. Commun. (2014). 10.1039/c4cc05237d.
[25] X. Kang, R. Yan, G. Yu, X. Pang, X. Liu, X. Li, L. Xiang, G. Huang, Iodine–mediated thiolation of substituted naphthols/naphthylamines and arylsulfonyl hydrazides via C (sp2)–H bond functionalization, J. Org. Chem. 79 (2014) 10605–10610.
[26] Q. Wu, D. Zhao, X. Qin, J. Lan, J. You, Synthesis of di(hetero)aryl sulfides by directly using arylsulfonyl chlorides as a sulfur source, Chem. Comm.. (2011). 10.1039/c1cc13633j.
[27] F. Xiao, H. Xie, S. Liu, G. Deng, Iodine-Catalyzed Regioselective Sulfenylation of Indoles with Sodium Sulfinates, Adv. Synth. Catal. 356 (2014) 364–368.
[28] W. Ge, Y. Wei, Iodine-catalyzed oxidative system for 3-sulfenylation of indoles with disulfides using DMSO as oxidant under ambient conditions in dimethyl carbonate, Green Chem 14 (2012) 2066–2070.
[29] W. Ge, X. Zhu, Y. Wei, Iodine-Catalyzed Selective Synthesis of 2-Sulfanylphenols via Oxidative Aromatization of Cyclohexanones and Disulfides, Adv. Synth. Catal 355 (2013) 3014–3021.

[30] S. Guo, Y. Yuan, J Xiang, Metal-free oxidative C (sp3)–H bond thiolation of ethers with disulfides, Org. Lett 15 (2013) 4654–4657.
[31] B. Du, B. Jin, P. Sun, Syntheses of Sulfides and Selenides through Direct Oxidative Functionalization of C (sp3)–H Bond, Org. Lett 16 (2014) 3032–3035.
[32] D. Equbal, A.G. Lavekar, A.K. Sinha, Cooperative catalysis by bovine serum albumin–iodine towards cascade oxidative coupling-C(sp2)–H sulfenylation of indoles/hydroxyaryls with thiophenols on water, Org. Bimol. Chem 14 (2016) 6111–6118.
[33] P. Sang, Z. Chen, J. Zou, Y. Zhang, K2CO3 promoted direct sulfenylation of indoles: a facile approach towards 3-sulfenylindoles, Green Chem 15 (2013) 2096–2100.
[34] S.K.R. Parumala, R.K. Peddinti, Iodine catalyzed cross-dehydrogenative C–S coupling by C(sp2)–H bond activation: direct access to aryl sulfides from aryl thiols, Green Chem 17 (2015) 4068–4072.
[35] G. Khalili, A new synthesis of $$\varvec $$-aryl uracils from aryl thiols and 6-amino uracils in the presence of NC, Mol. Divers 20 (2016) 963–968.
[36] Y. Siddaraju, K.R. Prabhu, Iodine Promoted Regioselective α-Sulfenylation of Carbonyl Compounds using Dimethyl Sulfoxide as an Oxidant, Org. Lett 18 (2016) 6090–6093, doi:10.1021/acs.orglett.6b03084.
[37] J.-.P. Wan, S. Zhong, L. Xie, X. Cao, Y. Liu, L. Wei, KIO3-catalyzed aerobic cross–coupling reactions of enaminones and thiophenols: synthesis of polyfunctionalized alkenes by metal-free C–H sulfenylation, Org. Lett 18 (2016) 584–587.
[38] X. Liu, R. Cheng, F. Zhao, D. Zhang-Negrerie, Y. Du, K. Zhao, Direct β-acyloxylation of enamines via PhIO-mediated intermolecular oxidative C–O bond formation and its application to the synthesis of oxazoles, Org. Lett. 14 (2012) 5480–5483.
[39] Y. Yuan, W. Hou, D. Zhang-Negrerie, K. Zhao, Y. Du, Direct oxidative coupling of enamines and electron-deficient amines: tBAI/TBHP-mediated synthesis of substituted diaminoalkenes under metal-free conditions, Org. Lett 16 (2014) 5410–5413.
[40] S. Zhong, Y. Liu, X. Cao, J.-.P. Wan, KIO3-Catalyzed Domino C(sp2)−H Bond Sulfenylation and C−N Bond Oxygenation of Enaminones toward the Synthesis of 3-Sulfenylated Chromones, ChemCatChem 9 (2017) 465–468, doi:10.1002/cctc.201601273.
[41] Y. Siddaraju, K.R. Prabhu, Iodine-Catalyzed Cross Dehydrogenative Coupling Reaction: sulfenylation of Enaminones Using Dimethyl Sulfoxide as an Oxidant, J. Org. Chem. 82 (2017) 3084–3093, doi:10.1021/acs.joc.7b00073.
[42] A.J. Rybarczyk-Pirek, M. Łukomska-Rogala, S. Wojtulewski, M. Palusiak, N-Oxide as a Proton Accepting Group in Multicomponent Crystals: x-ray and Theoretical Studies on New p-Nitropyridine-N-oxide Co-Crystals, Cryst. Growth Des 15 (2015) 5802–5815, doi:10.1021/acs.cgd.5b01177.
[43] J. Hernández-Paredes, R.C. Carrillo-Torres, A.A. López-Zavala, R.R. Sotelo-Mundo, O. Hernández-Negrete, J.Z. Ramírez, M.E. Alvarez-Ramos, Molecular structure, hydrogen-bonding patterns and topological analysis (QTAIM and NCI) of 5-methoxy-2-nitroaniline and 5-methoxy-2-nitroaniline with 2-amino-5-nitropyridine (1:1) co-crystal, J. Mol. Struct. 1119 (2016) 505–516, doi:10.1016/j.molstruc.2016.05.012.
[44] E. Bosch, N.P. Bowling, J. Darko, The Power of Nonconventional Phenyl C–H•••N Hydrogen Bonds: supportive Crystal-Packing Force and Dominant Supramolecular Engineering Force, Cryst. Growth Des 15 (2015) 1634–1641, doi:10.1021/cg5014076.
[45] G. Singh, J. Sindhu, V.Kumar Manisha, V. Sharma, S.K. Sharma, S.K. Mehta, M.H. Mahnashi, A. Umar, R. Kataria, Development of an off-on selective fluorescent sensor for the detection of Fe3+ ions based on Schiff base and its Hirshfeld surface and DFT studies, J. Mol. Liq (2019) 296, doi:10.1016/j.molliq.2019.111814.
[46] R. Kataria, D. Vashisht, J. Sindhu, S. Sharma, S.K. Mehta, R. Kumar, S.C. Sahoo, S. kumar, F. Qu, F.A. Afkhami, A. Gupta, Crystal structure, Hirshfeld surface, DFT and BSA binding studies of dihydropyrazole-1-thiocarboxamides, J. Mol. Struct. 1196 (2019) 662–675, doi:10.1016/j.molstruc.2019.06.100.
[47] A. Chaudhary, J.M. Khurana, G. Khanna, M. Saroha, A Catalyst-Free Domino Protocol for the Chemoselective Synthesis of Multifunctionalised Pyrroles in Aqueous Media via Nitroketene-N, S-Acetal Chemistry, ChemistrySelect 3 (2018) 6334–6337.
[48] M. Saroha, K. Meena, J.M. Khurana, PPh3 Mediated Stereoselective Synthesis of 4-Fumarate Substituted 3-AcylCoumarins: a Cascade Reaction of 3-Acyl Coumarin with Alkyne Derivatives, Chem.Select 3 (2018) 5905–5909.
[49] M. Saroha, G. Bartwal, J.M. Khurana, Transition metal free K2CO3 mediated thioarylation, selenoarylation and arylation of 2-aminomaleimides at ambient temperature, Tetrahedron 75 (2019) 130486.
[50] H. Singh, J. Sindhu, J.M. Khurana, Synthesis of biologically as well as industrially important 1,4,5-trisubstituted-1,2,3-triazoles using a highly efficient, green and recyclable DBU-H<inf>2</inf>O catalytic system, RSC Adv 3 (2013), doi:10.1039/c3ra44440f.
[51] M. Nardelli, PARST95 - an update to PARST: a system of Fortran routines for calculating molecular structure parameters from the results of crystal structure analyses, J. App. Cryst. 28 (1995) 659, doi:10.1107/S0021889895007138.
[52] R. Taylor, O. Kennard, Comparison of X-ray and neutron diffraction results for the N-H ···O=C hydrogen bond, Acta Crystallogr. Sect. B 39 (1983) 133–138, doi:10.1107/S0108768183002116.
[53] J. Martínez, Local reactivity descriptors from degenerate frontier molecular orbitals, Chem. Phys. Lett 478 (2009) 310–322, doi:10.1016/j.cplett.2009.07.086.
[54] M.N. Arshad, A.-A.M. Al-Dies, A.M. Asiri, M. Khalid, A.S. Birinji, K.A. Al-Amry, A.A.C. Braga, Synthesis, crystal structures, spectroscopic and nonlinear optical properties of chalcone derivatives: a combined experimental and theoretical study, J. Mol. Struct. 1141 (2017) 142–156, doi:10.1016/j.molstruc.2017.03.090.
[55] F. Zielinski, V. Tognetti, L. Joubert, Condensed descriptors for reactivity: a methodological study, Chem. Phys. Lett 527 (2012) 67–72, doi:10.1016/j.cplett.2012.01.011.
[56] T.B. Tai, V.T.T. Huong, M.T. Nguyen, Theoretical Design of π-Conjugated Heteropolycyclic Compounds Containing a Tricoordinated Boron Center, J. Phys. Chem. C. 117 (2013) 14999–15008, doi:10.1021/jp4049154.
[57] P.K. Chattaraj, Chemical Reactivity and Selectivity: Local HSAB Principle *versus* Frontier Orbital Theory, J. Phys. Chem. A. 105 (2001) 511–513, doi:10.1021/jp003786w.
[58] R. Balawender, P. Geerlings, DFT-based chemical reactivity indices in the Hartree-Fock method. II. Fukui function, chemical potential, and hardness, J. Chem. Phys. 123 (2005) 124103, doi:10.1063/1.2012330.
[59] L.R. Domingo, E. Chamorro, P. Pérez, Understanding the reactivity of captodative ethylenes in polar cycloaddition reactions. A theoretical study, J. Org. Chem. (2008). 10.1021/jo800572a.
[60] C. Morell, A. Grand, A. Toro-Labbé, New Dual Descriptor for Chemical Reactivity, J. Phys. Chem. A. 109 (2005) 205–212, doi:10.1021/jp046577a.
[61] P. Sjoberg, P. Politzer, Use of the electrostatic potential at the molecular surface to interpret and predict nucleophilic processes, J. Phys. Chem. 94 (1990) 3959–3961.
[62] F. Weinhold, C.R. Landis, E.D. Glendening, What is NBO analysis and how is it useful? Int. Rev. Phys. Chem 35 (2016) 399–440, doi:10.1080/0144235X.2016.1192262.
[63] M. Nakano, H. Fujita, M. Takahata, K. Yamaguchi, Theoretical study on second hyperpolarizabilities of phenylacetylene dendrimer: toward an understanding of structure-property relation in NLO responses of fractal antenna dendrimers, J. Am. Chem. Soc. 124 (2002) 9648–9655, doi:10.1021/ja0115969.
[64] O.V. Dolomanov, L.J. Bourhis, R.J. Gildea, J.A.K. Howard, H. Puschmann, OLEX2: a complete structure solution, refinement and analysis program, J. Appl. Crystallogr. 42 (2009) 339–341, doi:10.1107/S0021889808042726.
[65] G.M. Sheldrick, Crystal structure refinement with SHELXL, Acta Crystallogr, Sect. C Struct. Chem 71 (2015) 3–8, doi:10.1107/S2053229614024218.
[66] S.K. Wolff, D.J. Grimwood, J.J. McKinnon, M.J. Turner, D. Jayatilaka, M.A. Spackman, CrystalExplorer (Version 3.1), Univ. West. Aust. (2012).
[67] M.J. Frisch, G.W. Trucks, H.B. Schlegel, G.E. Scuseria, M.A. Robb, J.R. Cheeseman, G. Scalmani, V. Barone, B. Mennucci, G.A. Petersson, Gaussian 09, rev, (2009).
[68] P.M.W. Gill, B.G. Johnson, J.A. Pople, M.J. Frisch, The performance of the Becke−Lee−Yang−Parr (B−LYP) density functional theory with various basis sets, Chem. Phys. Lett 197 (1992) 499–505.
[69] N.M. O'Boyle, A.L. Tenderholt, K.M. Langner, Cclib: a library for package-independent computational chemistry algorithms, J. Comput. Chem. (2008). 10.1002/jcc.20823.
[70] L.R. Domingo, M. Ríos-Gutiérrez, P. Pérez, Applications of the conceptual density functional theory indices to organic chemistry reactivity, Molecules. (2016). 10.3390/molecules21060748.
[71] L.R. Domingo, Molecular electron density theory: a modern view of reactivity in organic chemistry, Molecules. (2016). 10.3390/molecules21101319.
[72] E.D. Glendening, A.E. Reed, J.E. Carpenter, F. Weinhold, NBO 3.0 Program Manual, Theor. Chem. Institute, Univ. Wisconsin, Madison, WI, 1990.
[73] M.D. Hanwell, D.E. Curtis, D.C. Lonie, T. Vandermeersch, E. Zurek, G.R. Hutchison, Avogadro: an advanced semantic chemical editor, visualization, and analysis platform, J. Cheminfo 4 (2012) 17.